Journal of Statistical Physics, Vol. 54, Nos. 5/6, 1989

Analogue Simulation of Quantum Mechanical Systems

N. G. Stocks,[1] C. J. Lambert,[1] and P. V. E. McClintock[1]

Received March 30, 1988; revision received August 1, 1988

An extension of the technique of analogue simulation to the treatment of quantum mechanical systems, based on an analogue variant of the method of stochastic quantization, is reported. The analogue stochastic quantization (ASQ) technique is introduced by application to the quantum harmonic oscillator, a particularly simple system for which all the answers are already known. ASQ measurements of the lowest eigenvalues and eigenfunctions of the latter system are presented and compared with theoretical predictions. The future potential of the ASQ technique in relation to some more complicated quantum systems of topical interest is discussed.

KEY WORDS: Analogue simulation; stochastic systems; noise; Langevin equations; stochastic quantization; density of states; spectral dimensionality.

1. INTRODUCTION

Experiments on noise-driven analogue electronic circuits can provide a useful method for finding approximate solutions of stochastic nonlinear differential equations. The technique, together with its advantages and disadvantages, has been reviewed in detail elsewhere[2]; briefly, it is as follows. An analogue electronic circuit is constructed to model the system of interest, and is then driven by additive or multiplicative, colored or quasiwhite noise from an external noise generator. The response of the circuit is then analyzed by a digital data processor so as to extract the statistical quantities of interest, such as distribution functions, correlation times, power spectra, or moments. Usually, such experiments are relatively

[1] Department of Physics, University of Lancaster, Lancaster, LA1 4YB, United Kingdom.

[2] For a recent review see, e.g., ref. 1, especially the chapters by L. Fronzoni (Chapter 8) and P. V. E. McClintock and F. Moss (Chapter 9).

0022-4715/89/0300-1397$06.00/0

822/54/5-6-19

quick and straightforward, both in design and execution, and lead to results that have a typical accuracy of a few percent. This remains true even in the cases of extremely complicated multidimensional systems for which analytic solutions are not available and where digital simulation techniques tend to be greedy of central processor time, even on very large computers.

All of the analogue modeling schemes of this kind reported to date[3] have, to our knowledge, been confined to classical systems or to quantum systems under conditions such that they are governed by classical equations. In what follows, we report a major extension of the technique, enabling it to be applied to quantum mechanical systems. The method exploits the close relationship that exists between the Langevin/Fokker–Planck and Schrödinger equations.[3,4] Thus, the quantum properties of a given system can be deduced from studies of the time evolution of the associated Langevin equation, which, in turn, can be modeled by the electronic analogue technique under discussion.

In Section 2 we review briefly the theoretical basis of the stochastic quantization technique and discuss how it can be applied to a particularly simple example of a quantum system, the one-dimensional quantum harmonic oscillator. The experimental application of the analogue modeling technique to this system is described in Section 3. The results obtained by this method are presented in Section 4, where they are compared with exact theoretical predictions. In Section 5 we discuss future possibilities and, in particular, the feasibility and utility of applying analogue stochastic quantization (ASQ) modeling to more complicated quantum mechanical systems for which exact analytic solutions are not available.

2. STOCHASTIC QUANTIZATION

Stochastic quantization[5,6] is an alternative to the more usual Monte Carlo method,[7–10] which uses a relaxation technique such as the Metropolis algorithm[11] to evaluate imaginary-time Feynman path integrals, by mapping a d-dimensional quantum system onto a $(d+1)$-dimensional classical system and evaluating *equilibrium* properties of the latter. In its simplest form,[4] for a single degree of freedom x, the technique starts from a stochastic differential equation of the Langevin type

$$\dot{x} = -\frac{\partial W}{\partial x} + \eta(t) \tag{1}$$

[3] The successful modeling of quantum systems by *mechanical* analogue simulation should also be noted: see, for example, He and Maynard.[2]

with $\langle \eta(t)\, \eta(t') \rangle = \sigma \delta(t-t')$. The equilibrium density $\rho_{eq} \sim e^{-2W/\sigma}$ can be used to reduce the Fokker–Planck equation for the nonequilibrium density $\rho(x, t) \sim \rho_{eq}^{1/2} \psi(x, t)$ to an imaginary-time Schrödinger equation of the form

$$-\frac{\partial \psi}{\partial t} = H\psi \tag{2}$$

where

$$H = -\frac{\sigma}{2}\frac{\partial^2}{\partial x^2} + V(x) \tag{3}$$

with $V(x)$ and $W(x)$ related by the Ricatti equation[4]

$$V = \frac{1}{2\sigma}\left(\frac{\partial W}{\partial x}\right)^2 - \frac{1}{2}\frac{\partial^2 W}{\partial x^2} \tag{4}$$

As a consequence, one can readily show that if $x = x_0$ at time $t = 0$, the probability that the solution of (1) takes the value x at time t is

$$\rho(x, t \mid x_0) = \phi_0(x) \sum_{m=0}^{\infty} \frac{\phi_m(x_0)\, \phi_m(x)}{\phi_0(x_0)} e^{-\lambda_m t} \tag{5}$$

where $\phi_m(x)$ is an eigenstate of H with eigenvalue λ_m. Thus, the statistical quantity $\rho(x, t \mid x_0)$ can yield information about the quantum mechanical system described by H. This analysis is readily generalized to systems with more than one degree of freedom. In this way, one can compute both ground-state and low-lying excited state properties of a d-dimensional quantum mechanical system from a knowledge of the *nonequilibrium* properties of a d-dimensional stochastic system. At the present time, a variety of hybrid techniques[5,6] are available for implementing the above formalism on a digital computer. However, to our knowledge, the only work to date on stochastic quantization using analogue simulation is our own preliminary ASQ work outlined below.

As well as probing the zero-temperature limit, the above technique can be used to determine finite-temperature properties through the relation

$$Z(\beta) = \int dx\, \rho(x, \beta \mid x) = \sum_{m=0}^{\infty} e^{-\lambda_m \beta} \tag{6}$$

where Z is the partition function of the single-particle quantum mechanical system at inverse temperature β. Thus, from the nonequilibrium properties of a stochastic differential equation, one obtains information about the finite-temperature equilibrium properties of a quantum mechanical system.

This provides a complementary technique to a better known Monte Carlo method,[10] which makes use of an isomorphism between a quantum statistical system and a classical "polymer" chain of N masses coupled by harmonic springs. The isomorphism is exact only in the limit $N \to \infty$, but, provided the temperature is not too low, accurate results can be still obtained for small values of N.

The results presented in this paper are aimed at checking the feasibility of the technique by applying it to a simple quantum mechanical system of known properties. The system we examine is a simple harmonic quantum oscillator of frequency ω_c, for which Eqs. (1) and (3) become

$$\dot{x} = -\omega_c x + \eta(t) \tag{7}$$

and

$$H = -\frac{\sigma}{2}\frac{\partial^2}{\partial x^2} + \frac{\omega_c^2}{\sigma}\frac{x^2}{2} - \frac{\omega_c}{2} \tag{8}$$

respectively. The introduction of dimensionless variables

$$y = (\omega_c/\sigma)^{1/2} x, \qquad \tau = \omega_c t$$

yields for Eq. (5)

$$\rho(y, \tau \mid y) = \pi^{-1/2} e^{-y^2} \sum_{m=0}^{\infty} A_m H_m^2(y)\, e^{-m\tau} \tag{9}$$

where $A_m = (2^m m!)^{-1}$ and $H_m(y)$ is a Hermite polynomial of degree m. The right-hand side of this equation can be summed[12] to yield

$$\rho(y, \tau \mid y) = [\pi(1 - e^{-2\tau})]^{-1/2} \exp -\frac{[y(1 - e^{-\tau})]^2}{1 - e^{-2\tau}} \tag{10}$$

In what follows, we present experimental measurements of the coarse-grained density $\bar{\rho}$ defined by

$$\bar{\rho}(y, \tau \mid y) = (\Delta y)^{-1} \int_{y - \Delta y/2}^{y + \Delta y/2} dy'\, \rho(y', \tau \mid y) \tag{11}$$

where $\Delta y \ll 1$. Results are presented for *finite* τ *only*, where one expects that the difference between ρ and $\bar{\rho}$ will vanish as $\Delta y \to 0$. This behavior is to be contrasted with the situation at $\tau = 0$, where Eq. (5) shows that, no matter how small Δy, $\bar{\rho}(y, 0 \mid y) = 1$, whereas $\rho(y, 0 \mid y)$ does not exist.

3. ANALOGUE MODELING OF THE QUANTUM HARMONIC OSCILLATOR

The Ornstein–Uhlenbeck process (7) was simulated by the bandwidth limiting of quasiwhite Gaussian noise, using the single, active, low-pass filter shown schematically in Fig. 1. A simple analysis of the circuit yields

$$\tau_I \dot{x} = -\omega_c x + \eta(t)$$

where we have put $\tau_I = r_1 C$ and $\omega_c = r_1/r_2$ to yield the desired time-scaled Langevin equation.

The stochastic driving force $\eta(t)$ was obtained from a Wandel & Goltermann model RG1 noise generator, which produces an accurately Gaussian noise voltage with a flat frequency response over the band range 0–100 kHz. Before application to the circuit, the noise voltage was filtered through another low-pass filter. This ensured that the noise had a well-defined correlation time τ_n with a correlation function

$$\langle \eta(t_1)\, \eta(t_2) \rangle = \frac{D}{\tau_n} \exp - \frac{|t_1 - t_2|}{\tau_n}$$

For reasons discussed elsewhere,[1,13] the Langevin equation was time scaled in the usual manner. This leads to the scaled noise intensity

$$D = \frac{\tau_n}{\tau_I} \langle V_n^2 \rangle$$

where $\langle V_n^2 \rangle$ is the mean square noise voltage, measured at the input to the circuit. Taking into account the time scaling, the dimensionless variables introduced in Section 2 become

$$y = (\omega_c/2D)^{1/2}\, x, \qquad \tau = (\omega_c/\tau_I)\, t$$

The factor of 2 appearing in the denominator of y results from the non-equivalence of σ with D. This can be shown by considering the correlation function in the white noise limit, in which case we obtain

$$\sigma = 2D$$

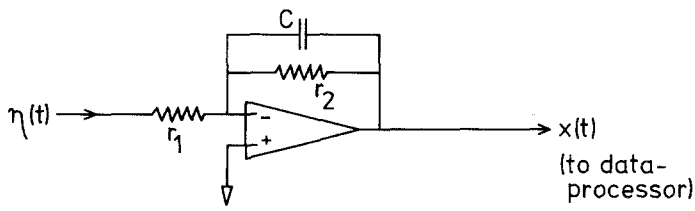

Fig. 1. Schematic diagram of the electronic circuit used to model Eq. (7).

The parameter values ω_c and D were chosen so as to optimize $x(t)$ for the circuit, the digitizer, and the data analysis procedure described below.

The computation of $\bar{\rho}(y, t \mid y)$ assumes the Markovianicity of the Langevin process. This is a valid assumption for the discretized version of $x(t)$ if $\tau_n \ll \tau_I$. For this reason typical values of τ_n and τ_I used where 20 μsec and 5 msec, respectively, thus yielding a ratio of $\tau_I/\tau_n \sim 250$.

Additional digital circuitry was incorporated to initialize the output of the circuit to a given value and to produce a triggering pulse for the computer used for data processing. This enabled the circuit to relax through the entire state space of interest during data acquisition. The typical mode of operation was as follows. First, a voltage pulse was sent to the circuit initializing its output to some large positive or negative value by charging the capacitor C. Synchronized with the trailing edge of this pulse, at the instant when the system was effectively "released," a trigger pulse was applied to the digitizer of a Nicolet 1180 or 1280 data processor, thus initiating a data acquisition sweep; immediately on completion of the sweep, the acquired $x(t)$ was analyzed, as described below. The sign of the charging pulses applied to C was alternately positive and negative, so as to cover the whole range of interest of x.

The successive sweeps of $x(t)$, typical examples of which are shown in Fig. 2, were analyzed to extract the coarse-grained return-time density $\bar{\rho}(x, t \mid x)$. The procedure for doing so was as follows. First the input $x(t)$ was digitized in both x and t, with 12-bit precision in x and into 256 or more time channels, separated by a sample interval typically of 80 μsec. The discretized $x(t)$ was placed in a block of memory for analysis. A number of different algorithms were investigated for extraction of $\bar{\rho}(x, t \mid x)$, but the most successful of them in practice, used for the results to be presented below, also turned out to be the simplest. The accessible range of positive and negative x was considered to be divided into 128 intervals, and each of these was examined in turn. For a particular interval, the program searched from $t = 0$ over increasing time until a count was found in that interval; the corresponding value of t was then regarded as the zero of time for that interval. Next, the program searched for returns to the interval; on each occasion that a return was found, it incremented the appropriate address in the memory block where the return-time density function for that value of x was being constructed. The search ceased after 128 sample intervals from the time origin had been examined. The next value of x was processed in a like manner, and so on, thus building up the required $\bar{\rho}(x, t \mid x)$ as a 128×128 point array. The next sweep of $x(t)$ was then digitized, and the whole process repeated. The sequence continued until the statistical quality of $\rho(x, t \mid x)$ was considered to be satisfactory.

In actual fact, the procedure for the choice of time origin was slightly

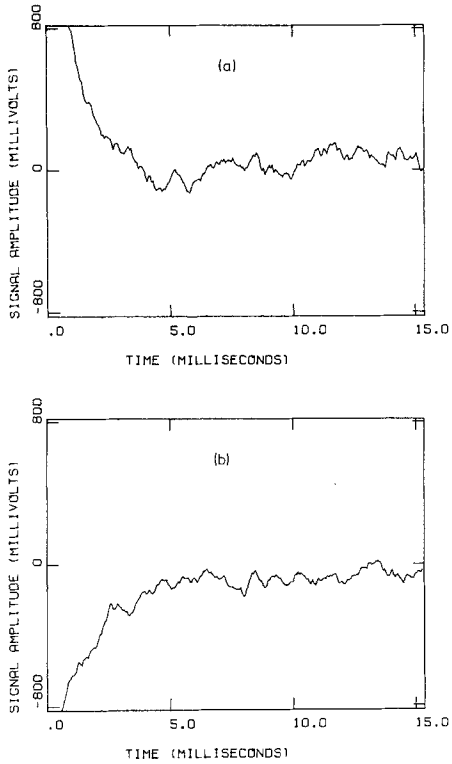

Fig. 2. Two examples of realizations of $x(t)$ from the output of the circuit in Fig. 1: (a) with an initializing pulse to make x positive; (b) with an initializing pulse to make x negative.

more complicated than described above. Alternatively, between pairs of positively and negatively initiated sweeps, the origin was chosen as *either* the first *or* the second occasion when $x(t)$ was found to be within the interval of interest. This procedure eliminated what would otherwise have been a biasing effect arising from the fact that the circuit operates continuously, rather than being "released" in turn at each chosen value of x.

Densities produced in this way required normalization to take account of the fact that, in general, the number of realizations of $\bar{\rho}(x, t \mid x)$ varied with x (because there were fewer of them at large values of x, where, on average, the system tended to drift rapidly toward decreasing $|x|$. Consequently, throughout the data acquisition sequence, a record was maintained of the number of realizations that had been analyzed for each value of x, thus creating a 128-point realization density in a separate memory block. Finally, the acquired $\bar{\rho}(x, t \mid x)$ was normalized by dividing it, for each value of t, by the realization density.

4. EXPERIMENTAL RESULTS AND COMPARISON WITH THEORY

The results presented below serve to demonstrate two important points. First, the analogue simulation yields accurate measurements of the return density $\rho(y, \tau \mid y)$; this is demonstrated by comparing experimental results for $\bar{\rho}(y, \tau \mid y)$ with the theoretical prediction for $\rho(y, \tau \mid y)$ given in Eq. (10). Second, quantum mechanical properties can be extracted from the experimental results; this is demonstrated by extracting the lower lying eigenfunctions and eigenvalues directly from the experimental data.

In order to compare experimental measurements of $\bar{\rho}$ with the theoretical prediction for ρ the experimental data are scaled such that, over the range of y and τ investigated, the volumes under the two curves are identical. Figure 3 shows the experimentally measured $\bar{\rho}(y, \tau \mid y)$, obtained from 10^5 realizations of $x(t)$. Figures 4 and 5 show sections through this two-dimensional density taken at constant τ and constant y, respectively. In these figures the dashed lines are experimental results for $\bar{\rho}$ and, for comparison, the solid lines show the theoretical values for ρ given by Eq. (10). These results show that, even for the shortest times illustrated, the differences between $\bar{\rho}$ and ρ are negligibly small. This agreement is

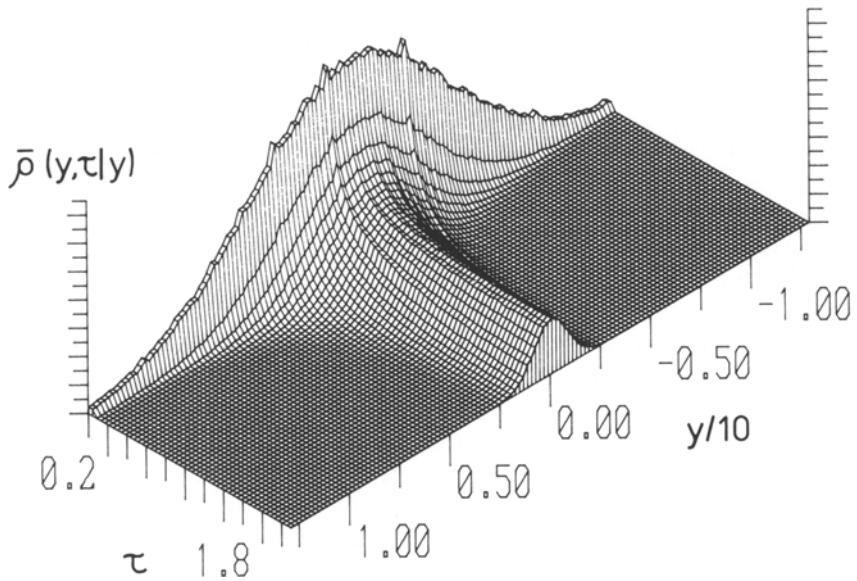

Fig. 3. The coarse-grained return-time density $\bar{\rho}(y, \tau \mid y)$, defined by Eq. (11), as measured experimentally for the circuit of Fig. 1.

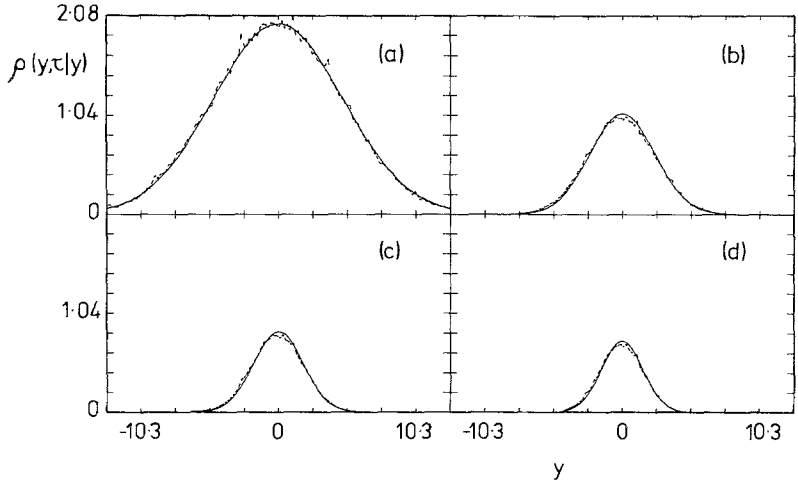

Fig. 4. Plots of the return density $\rho(y, \tau \mid y)$ versus y for fixed values of τ: (a) $\tau = 0.0833$; (b) 0.208; (c) 0.333; (d) 0.458. The solid curves represent the exact theory [Eq. (10)] and the dashed curves represent the experimental measurements of $\tilde{\rho}(y, \tau \mid y)$ for the circuit of Fig. 1.

also evident in Fig. 6, which shows the "partition function" $Z(\tau) = \int dy\, \rho(y, \tau \mid y)$ introduced in Eq. (6). In this figure the experimental and theoretical curves are almost indistinguishable. These results clearly demonstrate that analogue simulation provides an accurate technique for determination of the return density $\rho(y, \tau \mid y)$. We now demonstrate that

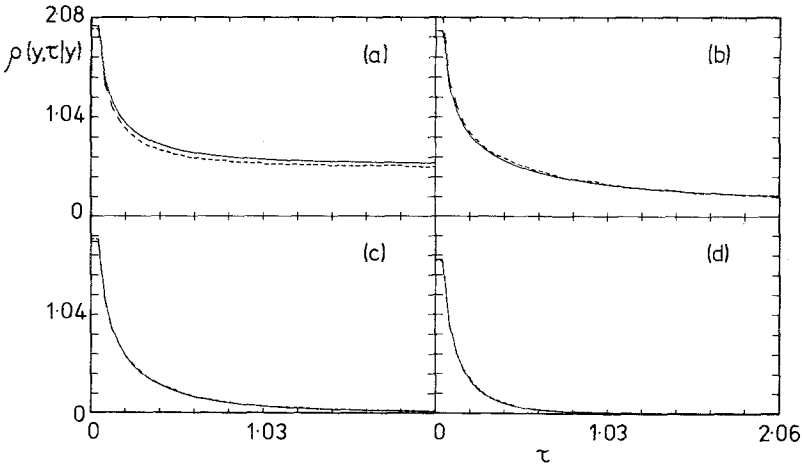

Fig. 5. Plots of the return density $\rho(y, \tau \mid y)$ versus τ for fixed values of y: (a) $y = 0.1$; (b) 1.1; (c) 2.1; (d) 3.1. The solid curves represent the exact theory [Eq. (10)] and the dashed curves represent the experimental measurements $\tilde{\rho}(y, \tau \mid y)$ for the circuit of Fig. 1.

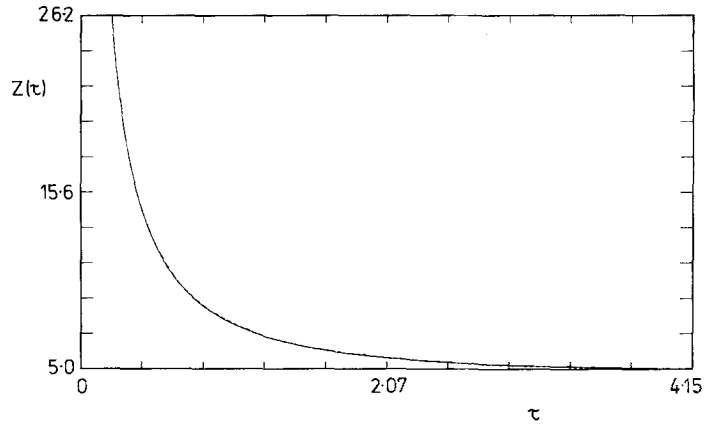

Fig. 6. The integrated density $Z(\tau)$ plotted against τ. The exact theory (solid curve) obtained by integration of (10) is compared to the experimentally measured curve (dashed) obtained by summing over y the coarse-grained return-time density $\bar{\rho}(y, \tau \mid y)$ shown in Fig. 3. The two curves are almost coincident.

quantum mechanical quantities such as energy level separations and eigenfunctions can be extracted from the experimental measurements of $\bar{\rho}$.

From the general expression (6), given the close agreement established above between ρ and $\bar{\rho}$, one can in principle obtain estimates for all of the level separations $\bar{\lambda}_m = \lambda_m/\hbar\omega_c$ between the lowest excited states and the ground state of the quantum system by fitting the function $1 + \sum_{m=1}^{\infty} \exp(-\bar{\lambda}_m \tau)$ to the experimental data for $Z(\tau)$. Here we have noted that in the mapping defined by Eqs. (1)–(4), the energy origin is

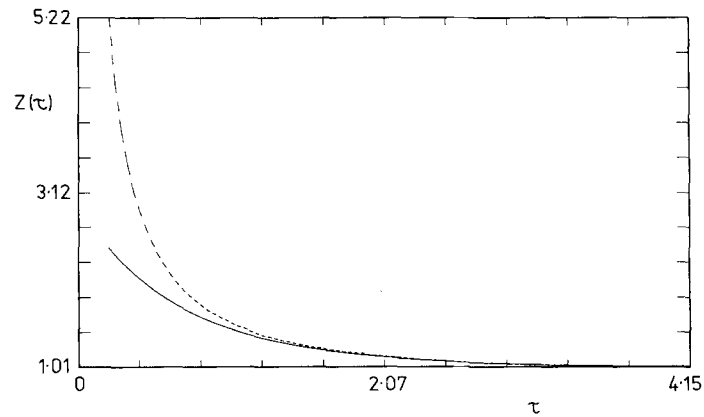

Fig. 7. The (normalized) experimental data of Fig. 6 (dashed curve) compared to a fit of (12) at large τ (solid curve) using $\bar{\lambda}_1 = 1.05$ and $\bar{\lambda}_2 = 1.93$.

necessarily chosen such that the ground-state energy of the quantum mechanical system is zero. In practice, an accurate fit to the experimental data is only possible at large times, where the exponentials $\exp(-\bar{\lambda}_m\tau)$ are well separated. For this reason only the lower $\bar{\lambda}_m$ are readily accessible. Figure 7 shows the result of a chi-squared fit of the function

$$f(\tau) = 1 + \exp(-\bar{\lambda}_1\tau) + \exp(-\bar{\lambda}_2\tau) \tag{12}$$

(solid line) to the experimental measurements (dashed line) of $Z(\tau)$ at large τ. The optimum values of $\bar{\lambda}_1$ and $\bar{\lambda}_2$ obtained from the fit are

$$\bar{\lambda}_1 = 1.05 \qquad \text{and} \qquad \bar{\lambda}_2 = 1.93$$

These are to be compared with the exact results of 1 and 2, respectively.

Given estimates for the eigenvalues $\bar{\lambda}_m$, the eigenfunctions themselves can readily be determined. Since $\bar{\lambda}_0$ is identically zero, the general expression (6) yields

$$\operatorname*{Lt}_{\tau\to\infty} \rho(y, \tau \mid y) = \phi_0^2(y) \tag{13}$$

Thus, the cross section at the largest value of τ shown in Fig. 3 is a plot of the ground-state intensity $\phi_0^2(y)$ of a quantum harmonic oscillator. From

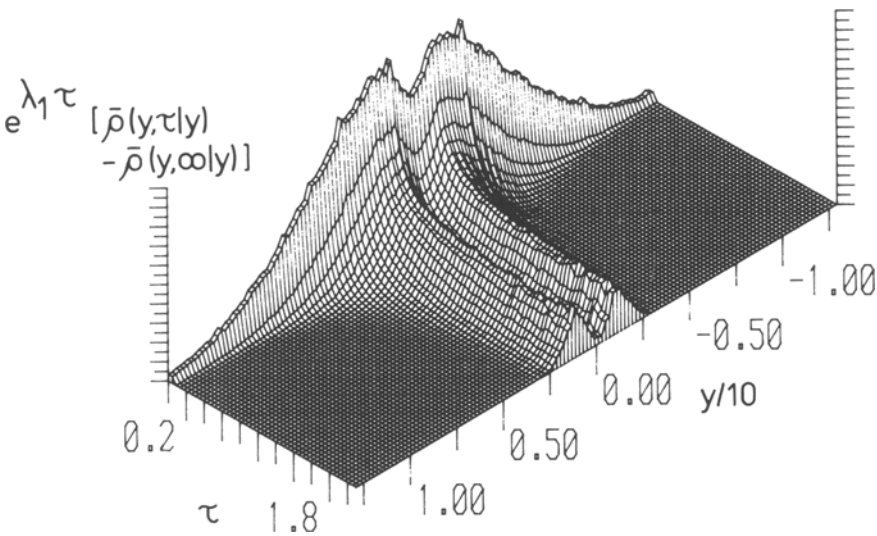

Fig. 8. The measured return-time density of Fig. 3, replotted according to Eq. (14): the stationary density at large τ has been subtracted, and all points have been multiplied by $\exp(\bar{\lambda}_1\tau)$, using the experimentally derived value of $\bar{\lambda}_1 = 1.05$. Under these conditions, as discussed in the text, the cross section in y tends toward the spatial intensity ϕ_1^2 as $\tau \to \infty$.

Eq. (2), one notes that the spatial intensity of the first excited state is obtained from the function

$$\rho^{(1)}(y, \tau \mid y) = [\exp(\bar{\lambda}_1 \tau)][\rho(y, \tau \mid y) - \phi_0^2(y)] \tag{14}$$

which satisfies

$$\operatorname*{Lt}_{\tau \to \infty} \rho^{(1)}(y, \tau \mid y) = \phi_1^2(y)$$

The spatial intensities of successively higher eigenstates can in principle be obtained from a sequence of such subtractions. In practice, accurate results are obtained only for the low-lying states, since errors arising from successive subtractions are compounded. Figure 8 shows experimental results for the quantity $\rho^{(1)}(y, \tau \mid y)$ obtained using the estimate $\bar{\lambda}_1 = 1.05$. The cross section at large τ clearly reflects the well-known spatial intensity of the first excited state of a quantum oscillator.

Finally, one notes that if τ is much less than the inverse level separation, the summation on the right-hand side of Eq. (6) can be replaced by an integral to yield

$$Z(\tau) = \int d\bar{\lambda}\, N(\bar{\lambda}) \exp(-\bar{\lambda}\tau) \tag{15}$$

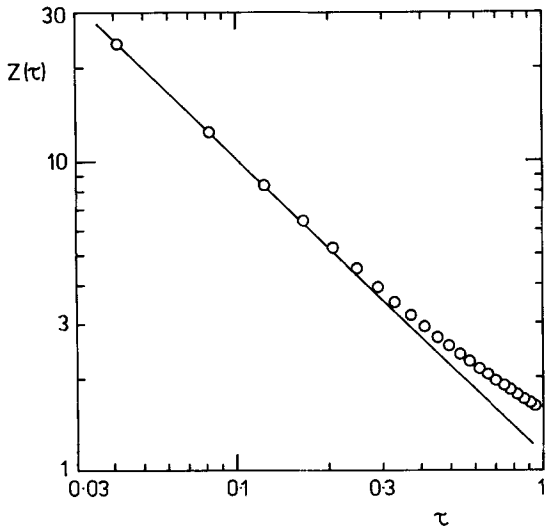

Fig. 9. A log-log plot of the integrated experimental density $Z(\tau)$ versus τ for small times τ. From the gradient (-0.97, which ≈ -1) of the line fitted at small τ, it may be inferred (correctly) that the density of states for the quantum harmonic oscillator at large energies is independent of energy.

where $N(\bar{\lambda})$ is the density of states at $\bar{\lambda}$. If $N(\bar{\lambda})$ varies like $\bar{\lambda}^P$, then this yields for small τ

$$Z(\tau) \sim \tau^{-(P+1)} \tag{16}$$

Figure 9 shows a log-log plot of the experimentally measured $Z(\tau)$ versus τ. For small τ, the measured slope (the line on the graph) of this is -0.97, yielding a value for P of 0.03. This derived value of $P \simeq 0$ reflects the well-known constant coarse grained density of states of the quantum harmonic oscillator.

5. DISCUSSION

The aim of this paper has been to demonstrate the feasibility of simulating quantum mechanical systems by the use of analogue electronic circuits. The above results clearly demonstrate that, from the long-time behavior of the return density ρ, the energies and eigenfunctions of the low-lying states are readily accessible. Futhermore, from the behavior of ρ at short times, the density of states $N(\bar{\lambda})$ can be extracted. In this initial investigation, we deliberately chose to examine the simplest of quantum mechanical systems. Having used this to establish the technique, we now envisage extending the method to more complex problems.

First one notes that it is relatively straightforward to extend the above simulation to encompass other single-degree-of-freedom systems whose quantum mechanical potential $V(x)$ is a polynomial in x, because in such cases the Riccatti equation (4) can easily be inverted to yield $W(x)$ for a given $V(x)$. The resulting Langevin equation will in general be a nonlinear stochastic equation with no exact analytic solution.

Second, by coupling together d electronic circuits of the kind discussed in this paper, one can extend the simulations to d-dimensional quantum mechanical systems.

Finally, it should also be possible to extend the technique to systems with complex quantum mechanical potentials, as follows. For a given $V(x)$ one can invert the Riccatti equation numerically and hence construct a numerical solution for the force term $f(x) = -\partial W/\partial x$ appearing in the Langevin equation (1). The force $f(x)$ can then be written directly onto an EPROM and inserted into the analogue circuit.[14]

We are currently aiming to use the latter version of the technique to examine the properties of disordered and self-similar structures. Examples of the latter are percolating structures near the percolation threshold where, at wavelengths less than the correlation length, the eigenstates are fractons[15] whose density of states varies with energy E as $N(E) \sim E^{(\bar{d}-2)/2}$,

with $\tilde{d}$ the spectral dimensionality. The analysis leading from Eq. (15) to Eq. (16) shows that the ASQ technique is ideally suited to the determination of spectral dimensionalities, because the experimentally accessible quantity $Z(\tau)$ yields $\tilde{d}$ immediately through the relation $Z(\tau) \sim \tau^{-\tilde{d}/2}$.

6. CONCLUSION

We have demonstrated that the ASQ technique can provide an accurate (to a few percent) description of the quantum harmonic oscillator; and we have shown how it can readily be extended to encompass other quantum systems as well. There is reason to believe that ASQ will prove a useful adjunct to more conventional methods of studying a variety of complex quantum mechanical systems of topical interest.

ACKNOWLEDGMENTS

We are indebted to Riccardo Mannella for a suggestion that led to the initiation of the studies described in this paper, to Charles Williams for help and advice at various stages, and to Frank Moss for his continuing encouragement. The work was supported by the Science and Engineering Research Council (U.K.).

REFERENCES

1. F. Moss and P. V. E. McClintock, eds., *Noise in Nonlinear Dynamical Systems: Vol. 3, Experiments and Simulations* (Cambridge University Press, 1988).
2. S. He and J. D. Maynard, *Phys. Rev. Lett.* **57**:3171 (1986).
3. N. G. van Kampen, *J. Stat. Phys.* **17**:71 (1977); H. Risken, *The Fokker–Planck Equation* (Springer, Berlin, 1984).
4. T. Schneider, M. Zannetti, and R. Badii, *Phys. Rev. B* **31**:2941 (1985).
5. S. Duane and J. B. Kogut, *Nucl. Phys. B* **275**:398 (1986).
6. S. Duane, A. D. Kennedy, B. J. Pendleton, and D. Roweth, to be published.
7. M. Creutz and B. Freedman, *Ann. Phys.* (N.Y.) **132**:427 (1981).
8. M. F. Herman, E. J. Bruskin, and B. J. Berne, *J. Chem. Phys.* **76**:5150 (1982).
9. J. A. Barker, *J. Chem. Phys.* **70**:2914 (1979).
10. M. J. Gillan, *Phys. Rev. Lett.* **58**:563 (1987).
11. N. Metropolis, A. W. Rosenbluth, M. N. Rosenbluth, A. H. Teller, and E. Teller, *J. Chem. Phys.* **21**:1087 (1953).
12. W. Horsthemke and R. Lefever, *Noise-Induced Transitions* (Springer, Berlin, 1984).
13. J. M. Sancho, R. Mannella, P. V. E. McClintock, and F. Moss, *Phys. Rev. A* **32**:3639 (1985).
14. K. Vogel, H. Risken, W. Schleich, M. James, F. Moss, R. Mannella, and P. V. E. McClintock, *Phys. Rev. A* **35**:463 (1987); *J. Appl. Phys.* **62**:721 (1987).
15. S. Alexander, J. Bernasconi, and R. Orbach, *Phys. Rev. B* **17**:4311 (1978).